Plume detachment from a magnetic nozzle

Christopher A. Deline,[1,a)] Roger D. Bengtson,[2] Boris N. Breizman,[2] Mikhail R. Tushentsov,[2] Jonathan E. Jones,[3] D. Greg Chavers,[3] Chris C. Dobson,[3] and Branwen M. Schuettpelz[4,b)]
[1]*University of Michigan, Ann Arbor, Michigan 48109, USA*
[2]*Institute for Fusion Studies, University of Texas at Austin, Austin, Texas 78712, USA*
[3]*Marshall Space Flight Center, Huntsville, Alabama 35805, USA*
[4]*University of Alabama at Huntsville, Huntsville, Alabama 35899, USA*

(Received 29 December 2008; accepted 16 January 2009; published online 12 March 2009)

High-powered electric propulsion thrusters utilizing a magnetized plasma require that plasma exhaust detach from the applied magnetic field in order to produce thrust. This paper presents experimental results demonstrating that a sufficiently energetic and flowing plasma can indeed detach from a magnetic nozzle. Microwave interferometer and probe measurements provide plume density, electron temperature, and ion flux measurements in the nozzle region. Measurements of ion flux show a low-beta plasma plume which follows applied magnetic field lines until the plasma kinetic pressure reaches the magnetic pressure and a high-beta plume expanding ballistically afterward. Several magnetic configurations were tested including a reversed field nozzle configuration. Despite the dramatic change in magnetic field profile, the reversed field configuration yielded little measurable change in plume trajectory, demonstrating the plume is detached. Numerical simulations yield density profiles in agreement with the experimental results. © *2009 American Institute of Physics*. [DOI: 10.1063/1.3080206]

I. INTRODUCTION

The magnetic nozzle is a critical component of some plasma propulsion systems that employ a strong guiding magnetic field to control plasma flow. A magnetic nozzle accelerates an incoming plasma flow by converting its internal energy into the kinetic energy of a directed jet. The magnetic nozzle also confines the plasma exhaust, limiting erosion and particle losses to facing surfaces. The ejected plasma must eventually break free from the applied magnetic fields in order to separate from the spacecraft and produce thrust. A commonly expressed concern regarding an applied magnetic field is that the field lines are closed; as a result, a plasma remaining attached (frozen) onto the field lines would produce no net thrust. This concern was succinctly voiced by Gerwin *et al.*[1] "…if the plasma were highly conducting, it would then have to follow the radially diverging magnetic field lines back around the field coils where it would ultimately deposit its momentum onto the vehicle, thereby negating the thrust." Plasma detachment has since been viewed as a key issue for plasma based propulsion systems using a magnetic nozzle for directed thrust.

It was thought early on that breaking the frozen-in constraint via recombination was the only solution to the detachment problem.[1] Alternatively,[2,3] the detachment issue can be resolved within the framework of ideal magnetohydrodynamics (MHD), where the magnetic fields can be stretched by currents in the plasma exhaust. This allows a plasma plume to detach together with the frozen-in magnetic field with a high efficiency. For a plasma flowing into a diverging magnetic nozzle, the plasma's directed kinetic energy density $W_k=\frac{1}{2}m_i n_i v^2$ decreases as the plasma flows downstream due to flux conservation. However, magnetic field energy density $W_B=B^2/2\mu_0$ decreases more quickly and thus β_k—the ratio of the plasma's kinetic to magnetic field energy density—will increase downstream,

$$\beta_k=\frac{\mu_o n_i m_i v^2}{B^2}=\left(\frac{v}{v_A}\right)^2. \tag{1}$$

Note that β_k, the notation for plasma beta used in this work, chacterizes the flow energy rather than the more commonly used thermal energy. In the MHD detachment scenario, when β_k becomes greater than unity (a condition equivalent to the flow velocity exceeding the Alfvén velocity $v_A=B/\sqrt{\mu_0 n_i m_i}$), the magnetic field lines remain frozen into the plasma as the flow stretches them to infinity. The magnetic field in separated plasma flow arises from internal plasma currents. This is a situation analogous to the solar wind flowing outward from the sun, carrying magnetic field with it.[4]

It is appropriate here to point out the difference between the detachment of plasma and the detachment of isolated charged particles. A single ion will readily escape from an applied magnetic field line if its gyroradius is greater than the characteristic spatial scale of the magnetic field[5] (i.e., the ion is "nonmagnetized"). For a sufficiently dense plasma, however, ions can only escape together with electrons in order to maintain the quasineutrality of the plasma. The electrons have a much smaller gyroradius than the ions and can remain tied to magnetic field lines even when the ions are not magnetized, which makes it more difficult for the ions to escape. These considerations motivate an experimental demonstration of MHD detachment involving a flowing plasma in a magnetic nozzle.

Several electric propulsion (EP) systems are being inves-

a)Electronic mail: cdeline@umich.edu. Present address: National Renewable Energy Laboratory, Golden, CO 80401.
b)Present address: Mantech SRS Technologies Inc., Huntsville, AL 35806.

 © 2009 American Institute of Physics

Downloaded 16 Apr 2009 to 128.83.61.67. Redistribution subject to AIP license or copyright; see http://pop.aip.org/pop/copyright.jsp

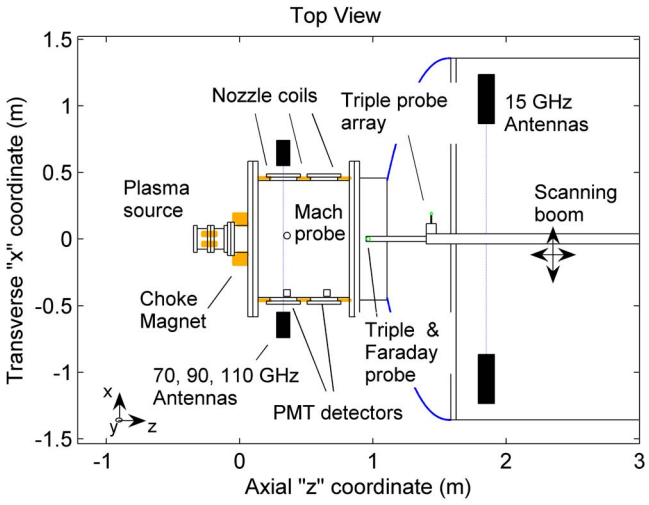

FIG. 1. (Color online) Top view of the experiment.

tigated for future exploration and orbit maintenance missions.[6–9] These systems utilize a plasma source with a magnetic field which shapes and confines the plasma plume. In particular, the variable specific impulse magnetoplasma rocket (VASIMR) concept provides motivation for the present work due to its high input power and high plasma density.[10] The plasma flow in VASIMR is produced by an ion cyclotron resonance heating (ICRH) module that deposits energy directly into ion gyromotion which is then converted to parallel flow energy in a magnetic nozzle. The high flow velocity coupled with high plasma density conditions is expected to meet the $\beta_k > 1$ condition.

An experiment has been performed at the NASA Marshall Space Flight Center, Huntsville, AL, to demonstrate a plasma detachment scenario for high density, high velocity plasma flows in a diverging magnetic nozzle. A 200 kW pulsed dc plasma source and 0.07 T peak magnetic nozzle field are employed such that the plume transitions from $\beta_k < 1$ to $\beta_k > 1$ in the experiment. High-vacuum conditions in a large vacuum chamber minimize charge exchange effects between flowing ions and background neutral particles. Several diagnostics are used to characterize the plasma flow along the length of the plume including measurements of ion flux, velocity, density, and electron temperature.

II. EXPERIMENTAL SETUP

Experiments were conducted in the large (2.75 m diameter $\times$ 5 m length) vacuum chamber at the NASA Marshall Propulsion Research Center. The large chamber with high pumping speed was chosen to minimize wall effects and to minimize ion-neutral charge exchange collisions. A detailed description of the experiment configuration has been presented previously.[11,12] A top view of the experiment is given in Fig. 1. Two diffusion pumps operate at a pumping speed of 100 000 l/s, keeping the chamber base pressure below 2×10^{-6} Torr. The dc plasma source is mounted near the front of the chamber. A series of three external nozzle coils wrapped around the chamber circumference and a small bore, high field "choke magnet" provides the magnetic nozzle field. The center of this choke magnet defines the origin of the chamber coordinate axis, with axial position $z=0$ m marking the peak field of the magnetic nozzle and coinciding with the center of the choke magnet.

Plasma was produced in a pulsed plasma washer gun[13] operating up to 200 kW. The washer gun consists of a 2 cm tall stack of molybdenum washers with an inner diameter (i.d.) of 5.0 mm and an outer diameter of 20 mm. A molybdenum anode and cathode at either end of the washer stack initiate the discharge arc. Isolation between the washers is provided by 1 mm thick boron nitride ceramic washers with an i.d. of 1 cm. Hydrogen and helium were used as feed gases, although other gases are possible. A plasma plume is created by discharging a capacitor bank charged to 270–300 V with a solid state control circuit. Typical pulse lengths were 3 ms in duration with a discharge voltage of 270–300 V and currents nearing 700 A. The pulse duration is several times longer than the ion travel time through the chamber, allowing the pulse to be considered steady state. Gas is delivered to the plasma source via a low pressure reservoir (9 psi absolute) and a Parker high speed puff valve remaining open for roughly 5 ms and triggered at the same time as the capacitor discharge.

The dc magnetic field of the nozzle is created by five separately powered magnet coils. The plasma gun coil has 300 turns and an i.d. of 5 cm, while the choke magnet coil has 166 turns with a 25 cm i.d. The final three nozzle magnet coils have a 91 cm i.d. and have 30, 21, and 15 turns, respectively. Nozzle coil currents were adjusted during the experiment to provide different magnetic configurations. The coil

TABLE I. Coil currents for the six magnetic nozzle configurations.

	I_{gun} (A)	I_{choke} (A)	I_{noz} No. 1 (A)	I_{noz} No. 2 (A)	I_{noz} No. 3 (A)
Config. 1	5	100	40	20	20
Config. 2	5	100	10	3	3
Config. 3	5	100	0	0	0
Config. 4	5	100	−20	0	0
Config. 5	5	100	−40	0	0
Config. 6	5	100	−40	−20	−20

Downloaded 16 Apr 2009 to 128.83.61.67. Redistribution subject to AIP license or copyright; see http://pop.aip.org/pop/copyright.jsp

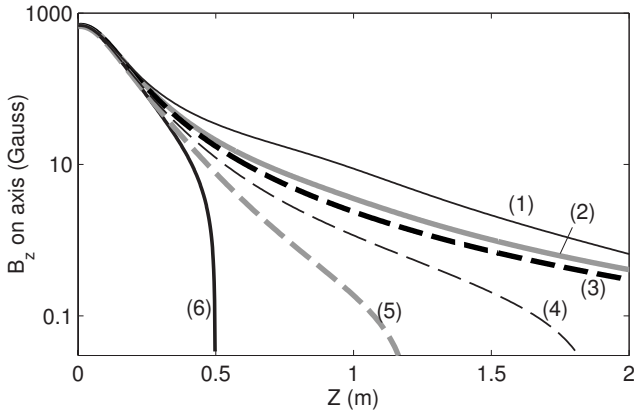

FIG. 2. Axial magnetic field on the experiment centerline for the coil currents listed in Table I.

currents and axial magnetic field strength[14] for the experiment centerline are shown in Table I and Fig. 2. A majority of shots were conducted using coil configuration "2," which approximates straight diverging magnetic field lines in the nozzle region. Experimental verification of the calculated magnetic field for configuration 2 was obtained using a three-axis magnetometer scanning along the experiment centerline. In the following discussion, magnetic fields refer to the vacuum magnetic field. We were unable to measure any plasma-current induced changes in the magnetic field due in part to low signal to noise ratio on B-dot probes and flux loops.

Neutral pressure in the vacuum chamber is measured with a Baratron 627B capacitance manometer and Granville–Phillips stabil-ion gauge. Neutral background pressure measurements taken near the plasma source show that the prepulse pressure is 2×10^{-6} Torr, reaching as high as 2×10^{-4} Torr after the pulse.

The composition of the neutral gas in the flowing hydrogen plasma is unknown, but assuming the worst possible case where hydrogen neutrals produce the pressure in the flowing plasma at the highest pressure measured, the mean free path for the resonant charge exchange processes, $p+\mathrm{H}\rightarrow\mathrm{H}+p$, is only 0.25 m. With this short mean free path, the plasma flow would quickly slow down as the plume travels downstream. We did not observe a flow deceleration and increased plasma density that could be attributed to ion neutral charge exchange. However, momentum exchange scattering from unlike-particle collisions cannot be explicitly ruled out in this experiment.

A. Plasma diagnostics

Our measurements in demonstrating plasma detachment provide radial profiles of ion flux and radial profiles of electron density at multiple axial positions. Both cylindrical triple probes[15,16] and guarded Faraday probes[17] were used to measure ion flux throughout the experiment via probe arrays, and a two-dimensional (2D) scanning stage. Two designs of Langmuir triple probes were used, one a smaller scanning probe with cylindrical stainless steel conductors with radius of 0.45 mm and height of 5 mm, and the other an array of larger cylindrical conductors with radius of 1.2 mm and height of 6 mm. Probe separation was 9 mm, small with respect to gradients in the plasma. All of the triple probes used in this experiment are oriented perpendicular to the plasma flow and mounted on a 2D insulated scanning boom allowing radial and axial scanning of the plume. The smaller Langmuir triple probe is located on the chamber centerline at the far upstream end of the diagnostics boom. The array of larger triple probes consists of six sets of triple probes arrayed vertically with the following y-coordinates: $y=\pm0.064$, ±0.191, and ±0.317 m. A battery string provides a -44 V bias for the double probe part of the triple probe. Ion saturation current is measured across a 10 Ω sensing resistor, and electron temperature is measured by the potential difference between the floating potential and the positive bias potential of the double probe. Ion saturation current for supersonic plasma flow is assumed to follow $I_{\mathrm{sat}}=S_p n_i q v_z$, where S_p is the frontal projected area of the cylindrical probe. All probes in this experiment are sized to collect ion current in the thin-sheath ($r_p>20\ \lambda_D$) regime. All probe measurements are optically isolated from chamber ground via an optical link and digitally recorded in a data acquisition system.

A guarded Faraday probe biased into ion saturation was also mounted at the end of the diagnostics boom. The Faraday probe is a circular planar collector surrounded by an annular guard ring biased to the same potential. Ion current is only measured at the center collector where the plasma sheath structure is uniform. The tungsten center collector has a diameter of 2.34 mm, and the surrounding stainless steel guard has inner and outer diameters of 5 and 6.35 mm, respectively. Isolation between the two pieces is maintained by an alumina ceramic tube. Ion current is collected by a -20 V bias and recorded over a 10 Ω sensing resistor.

Microwave interferometer systems at two axial locations provide spatial and temporal electron density measurements. A polychromatic quadrature interferometer is used that operates simultaneously at 70, 90, and 110 GHz.[18] This instrument is positioned near the nozzle entrance, 0.33 m downstream from the choke magnet. The spatial resolution for this interferometer is 0.015 m, with a minimum sensitivity of 10^{16} m^{-3} over the 1 m path length. This interferometer can be translated vertically, providing different chord measurements over several plasma shots.

A second interferometer system is mounted inside the vacuum chamber at $z=1.85$ m. This 15 GHz quadrature interferometer[19] provides a minimum sensitivity of $n_e=10^{15}$ m^{-3} for line-integrated measurements along the 1.7 m path length. Its two independent interferometer chords have one chord on the axial centerline and one positioned below it, at $y=-0.3$ m. This two-chord configuration allows a limited two-point density profile measurement for every plasma shot. Calibration of all interferometer systems was conducted daily, providing estimates of random and systematic error due to beam reflection and detector voltage drift.[18]

Interferometer density measurements are performed in two ways. Independent density profiles are obtained by vertical translation of the polychromatic interferometer over several plasma shots. An Abel inversion[20,21] is performed to

Downloaded 16 Apr 2009 to 128.83.61.67. Redistribution subject to AIP license or copyright; see http://pop.aip.org/pop/copyright.jsp

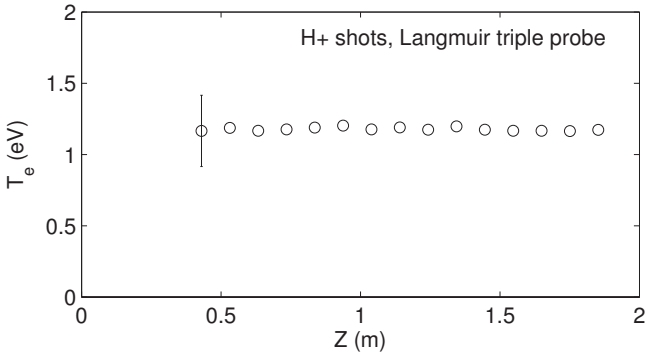

FIG. 3. Electron temperature measurements as a function of axial distance on the centerline.

transform the several line integral density measurements into a vertical electron density profile at the interferometer's axial position. A second density measurement method compares an interferometer's output with flux probe measurements performed along the interferometer chord. Assuming a radially uniform velocity profile, a high accuracy density profile is obtained over multiple shots.[22] Density profiles obtained with these two different methods compared favorably.

Triple-probe measurements[15] of electron temperature gave $T_e=1.2$ eV $\pm 20\%$ in hydrogen and $T_e=1.4\pm 20\%$ in helium with no evidence of spatial or temporal variation, as is shown in Fig. 3. Electron temperature is assumed here to follow standard triple-probe T_e analysis[15] where $T_e(\mathrm{eV})=V_{12}/\ln 2$ and V_{12} is the voltage difference between floating potential and the potential of the positive side of a floating double probe. When used to measure a flowing plasma with Mach number of >1, the standard triple-probe analysis is known to overestimate electron temperature.[23,24] Numerical simulations were conducted to address this issue,[25] with the result that simulated T_e error for these particular conditions is less than 15%, which is within measurement error bars. Plasma flow effects on triple-probe T_e measurements can thus be neglected here.

Plasma flow velocity is estimated with a variety of techniques: Mach probe, flux probe, and time of flight measurements. The Mach probe used in this experiment has one upstream facing pin and one downstream facing pin, each with diameter of 1 mm, separated by a dielectric barrier. It is positioned in the chamber at $z=0.33$ m near the axial centerline, $r=0$. The ratio of upstream/downstream ion currents was reduced to a Mach number following the work by Gunn.[26] The Mach number in the plume was measured to be $M=1.1\pm 15\%$, where

$$M=\frac{v}{c_s}=v\left(\frac{kT_e+kT_i}{m_i}\right)^{-1/2}. \tag{2}$$

We have no measurements of ion temperature and assume that it is equal to the electron temperature because of the Coulomb collisions in the plasma source. These assumptions contribute to uncertainty in the final Mach probe velocity measurement.

A second estimate of plasma velocity depends on two photomultiplier tubes (PMTs) separated by $\Delta z=0.3$ m and

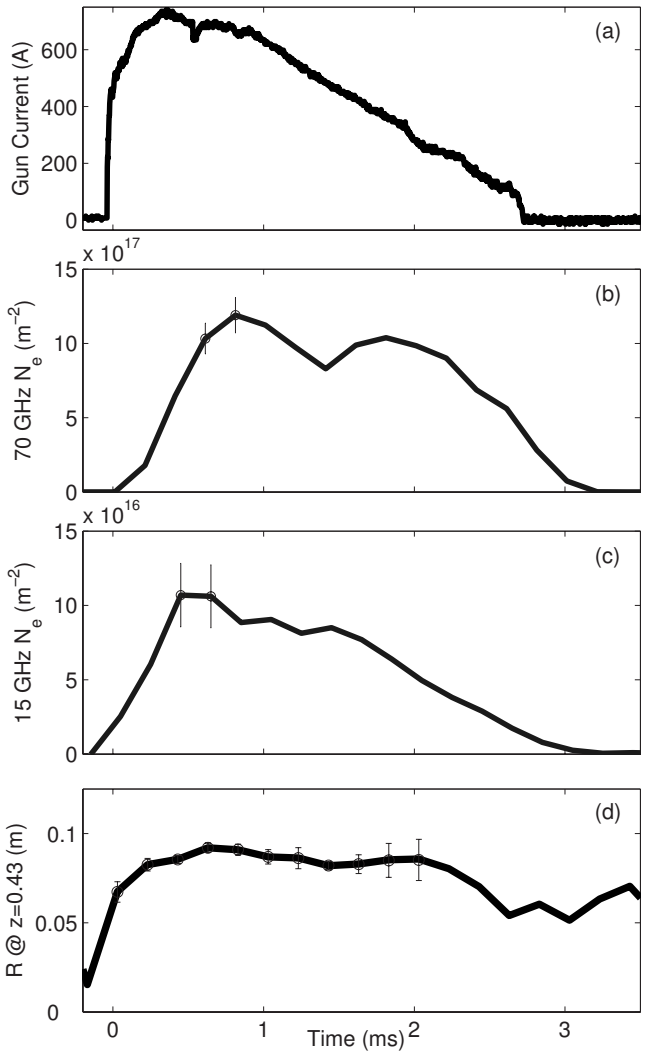

FIG. 4. (a) Plasma source discharge current during H_2 shots with magnet configuration 2. Discharge voltage for this typical shot was 270 V. (b) 70 GHz interferometer line integral density measurement at $z=0.33$ m. (c) 15 GHz interferometer line integral density measurement at $z=1.85$ m. (d) Column radius R measurement from probe scan at $z=0.43$ m. The plume averaged 0.085 m half-maximum radius at $z=0.43$ m. Error bars were determined by Monte Carlo analysis.

centered at $z=0.48$ m. The time delay between similar features on the PMT signals provides a flow velocity measurement averaged over 0.3 m. These devices are located outside the vacuum chamber and equipped with focusing optics to limit the view in the axial direction to 5 mm. This approach has been considered before for ion velocity measurements of an arcjet thruster.[27] The uncertainty for this method is expected to be around $\pm 40\%$ due to the velocity of the plasma flow relative to the feature size of the optical measurements. A similar time-of flight measurement was conducted by looking at the response from two axially separated Langmuir probes. The two probes were separated by $\Delta z=0.47$ m and were scanned axially on the 2D translation stage.

The third measurement of plasma flow velocity comes from the comparison of ion flux with interferometer electron density. Saturation current to a planar probe for directed ion flow in the thin-sheath limit is $I_i^{\mathrm{sat}}=S_p n_i q v_z$ and therefore knowledge of $n_e=n_i$ directly leads to an estimate of ion ve-

Downloaded 16 Apr 2009 to 128.83.61.67. Redistribution subject to AIP license or copyright; see http://pop.aip.org/pop/copyright.jsp

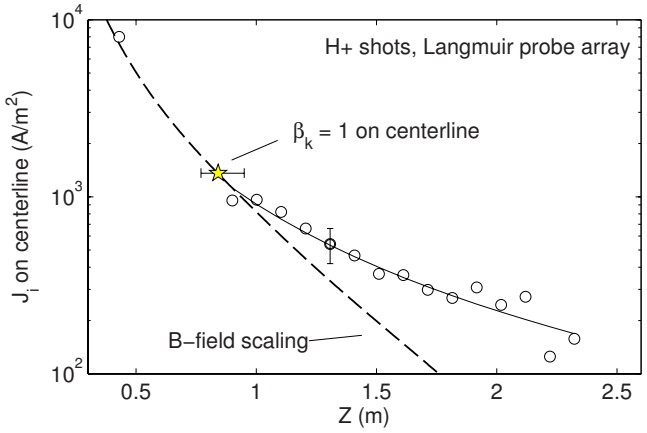

FIG. 5. (Color online) Ion flux (current density) on the experiment centerline for hydrogen shots, magnet configuration 2. *B*-field scaling (– –) assumes ions following *B*-fields according to Eq. (5).

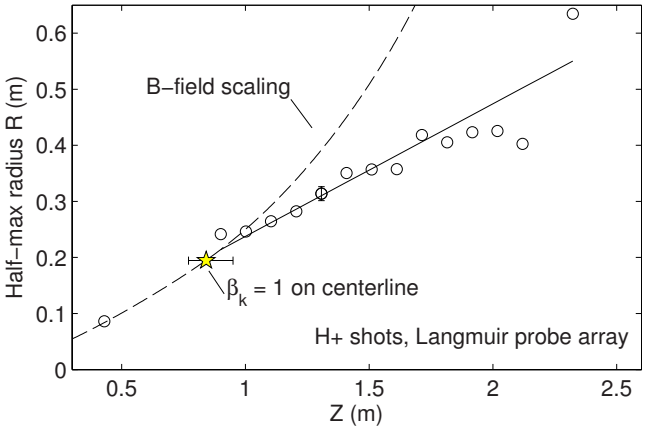

FIG. 6. (Color online) Plume radius for hydrogen shots at multiple axial positions. Plasma $\beta_k=1$ location is shown for the experiment centerline. B-field scaling (– –) assumes ions following *B*-fields according to Eq. (4).

locity. Sources of error in this method include an assumption of Gaussian radial density distribution, quasineutrality, and uniform velocity radial distribution. Measurements of plasma velocity are estimated to have error of the order of 30%. In general, the three velocity measurements were in good agreement in this experiment.

III. EXPERIMENTAL RESULTS

The plasma source is operated with either H_2 or He as a feed gas and with the magnetic nozzle in one of the configurations "1"–"6." A typical trace of plasma gun current and interferometer output for a plasma shot using H_2 feed gas and nozzle configuration 2 is shown in Fig. 4. Probe and interferometer scans are conducted over multiple plasma pulses to provide radial and axial profiles of plasma flux, T_e, v_z, and n_e. These scans allow measurements to be made for plasma beta: $0.1<\beta_k<10$.

A. Magnet configuration 2

In magnet configuration 2 (Fig. 2) the diverging vacuum magnetic field lines were nearly straight in the magnetic nozzle section using both hydrogen and helium gases.

1. Flux profiles

Axial scans of ion flux J_i are measured on the experiment centerline with the guarded Faraday probe and Langmuir triple-probe array. The probe array provides a radial distribution of ion flux due to the six radially separated probes at axial positions between $z=0.90$ m and $z=2.4$ m. All ion flux profiles approximately followed a Gaussian distribution:

$$J_i(r,z) = v_z e n_{\max}(z) e^{-(r^2/R(z)^2)\ln 2}, \tag{3}$$

where the plume width is the radius at half maximum, $R(z)$. The total ion current I_i through a measurement plane is obtained by a 2D integral of ion flux. Centerline ion flux, plume width, and total ion current for hydrogen gas averaged over the shot are plotted in Figs. 5–7. We also plot the ion flux J_i and plume width R assuming the ions are tied to the vacuum magnetic field lines. That is,

$$R(z)/R_0 = \sqrt{B_{z,0}/B_z(z)} \tag{4}$$

and

$$J_i(z)/J_0 = B_z(z)/B_{z,0}, \tag{5}$$

where subscript "0" denotes conditions at the farthest upstream probe measurement $z=0.43$. Also plotted in Figs. 5 and 6 are estimates of locations where $\beta_k=1$ on the experiment centerline, based on local velocity and density measurements and vacuum magnetic field. In the MHD detachment scenario, $\beta_k=1$ is the approximate position where the plume separates from applied magnetic field lines. This condition is consistent with the data. Trend lines shown in Figs. 5 and 6 are least-squares fit to experiment data. In the case of plume width data in Fig. 6 the best fit is linear, while Fig. 5 has a least-squares fit of the form $y=C_1x^{-C_2}$, where $C_2=2.0$. Note that the plasma flow is tied to the magnetic field lines from our first measurements at $z=0.43$ to the $\beta_k=1$ point on the centerline. After the $\beta_k=1$ point, the flow deviates from the magnetic field scaling reference curve.

A similar experiment was conducted using magnetic configuration 2 with helium feed gas instead of hydrogen.

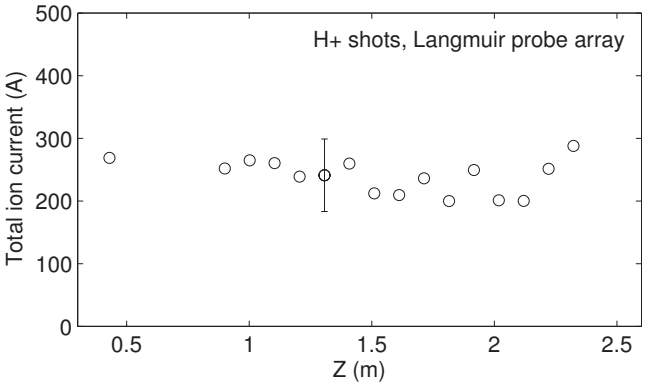

FIG. 7. The total ion current I_i for hydrogen shots based on a 2D integral of the Gaussian radial ion flux distribution.

Downloaded 16 Apr 2009 to 128.83.61.67. Redistribution subject to AIP license or copyright; see http://pop.aip.org/pop/copyright.jsp

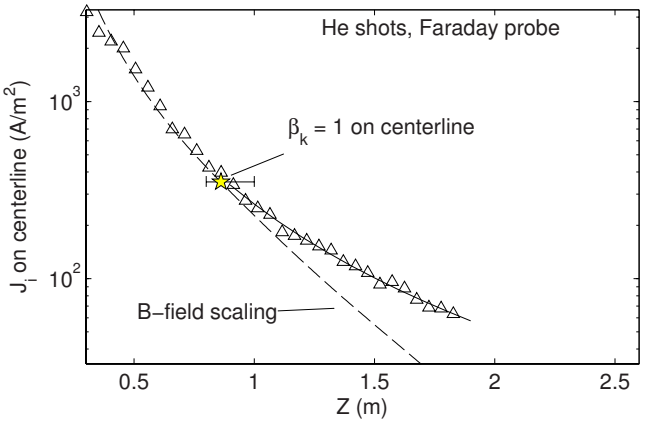

FIG. 8. (Color online) Ion flux (current density) J_i on the experiment centerline measured with the Faraday probe for He shots.

Only the guarded Faraday probe was available to provide centerline ion flux, so plume width and total ion current measurements are not available. Figure 8 shows results of the Faraday probe axial scan along with a reference curve for frozen flow scaling [Eq. (5)] and the estimated position of $\beta_k > 1$ detachment on the experiment centerline. A least-squares fit of the form $y = C_1 x^{-C_2}$ is plotted with the data where $C_2 = 2.37$. The same characteristics as noted for a hydrogen plume are visible. On the centerline the flux is tied to the applied magnetic field until the plasma β_k is greater than 1. After the transition the flow is no longer tied to the applied magnetic field and expands at a lower rate than the magnetic field expansion.

2. Density profiles

Radial profiles of electron density in the hydrogen plumes were obtained with a vertical scan of the polychromatic microwave interferometer at $z = 0.33$ m in 13 mm steps. After Abel inversion, the radius of the Gaussian density profile was found to be 48 ± 6 mm, in agreement with the width measured from the flux profile to within error bars. The peak of the Gaussian density profile at $z = 0.33$ m was 1×10^{19} m$^{-3} \pm 13\%$. At the downstream two-channel interferometer ($z = 1.85$ m), the two interferometer line averaged chord densities were consistent with a Gaussian density profile with width of $R = 0.45$ m and a peak plasma density of $n_e = 1 \times 10^{17}$ m$^{-3} \pm 20\%$. Flux probe scans at the same position yielded results consistent with this plume width.

3. Velocity

Hydrogen ion velocity is measured by three independent methods, as shown in Fig. 9. Mach probe measurements at $z = 0.33$ m give an ion Mach number of $M = 1.1 \pm 0.2$, which for $T_e = T_i = 1.2 \pm 0.2$ eV yields $v_z = 12-19$ km/s. Assuming an ion temperature of $T_i \approx 0$ yields the lower end of the v_z estimate, while a $T_i = T_e$ assumption yields the upper end of the velocity estimate. The high collisionality in the source leads us to prefer the higher flow velocity. Time of flight analysis between two photomultipliers at $z = 0.33$ m and $z = 0.63$ m suggests an average $v_z = 15 \pm 5$ km/s between the two PMTs. Due to the nature of this diagnostic, the measurement is an average velocity between the two stationary detectors. A third measurement at the interferometer locations, $z = 0.43$ m and 1.85 m, comes from flux measurements using probes and the electron density from the probe measurement. The centerline ion flux combined with the n_e profile from the interferometers results in a flow velocity of $v_z = 17 \pm 5$ km/s. All three velocity techniques combine to suggest a constant hydrogen velocity of 16 ± 5 km/s throughout the experiment. We do not observe flow acceleration by the ambipolar electric field

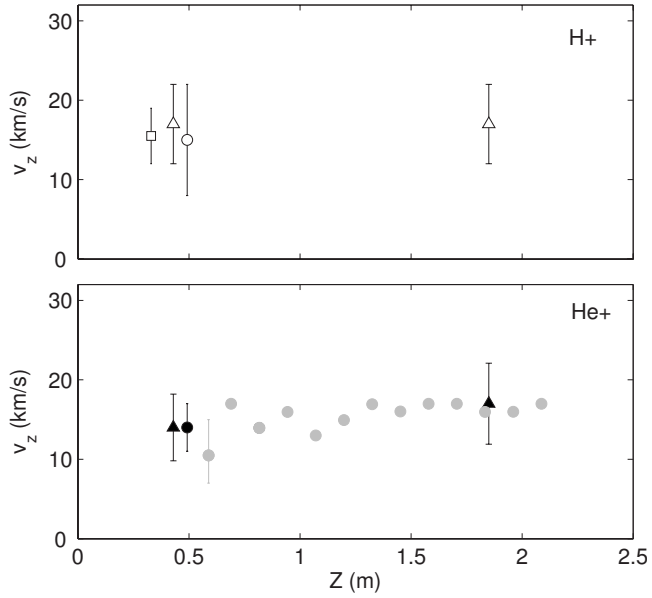

FIG. 9. Velocity measurements in hydrogen (top) and helium (bottom). □: Mach probe measurements; △: flux probe measurements; ○: time of flight measurements. Grey datapoints represent scanning probe time of flight measurements.

$$E = \frac{T_e}{e}\frac{\partial}{\partial z}\ln n$$

despite the decrease in electron density by roughly a factor of 100. The constant flow velocity could be due to charge exchange collisions slowing down the flow. It should also be noted that the widths of the Gaussian profiles of density and ion flux were the same within error limits, suggesting that flow velocity was constant in radius.

Helium velocity measurements were measured using a time of flight technique and measurements of plasma flux and electron density profiles, as shown in Fig. 9. An additional time of flight axial scan was also performed with helium shots using the relative response of two axially separated Langmuir probes. The two probes maintained a fixed separation (0.3 m), while the entire apparatus was adjusted axially giving an axial scan of velocity. This axial scan shows a slight increase in velocity with axial position, but well within measurement error bars. Therefore, any definitive measurement of flow acceleration or deceleration within the experiment for H_2 or He shots is obscured by measurement uncertainties.

Velocity measurements in helium gave a constant velocity of 15 ± 5 km/s, somewhat faster than might be expected

Downloaded 16 Apr 2009 to 128.83.61.67. Redistribution subject to AIP license or copyright; see http://pop.aip.org/pop/copyright.jsp

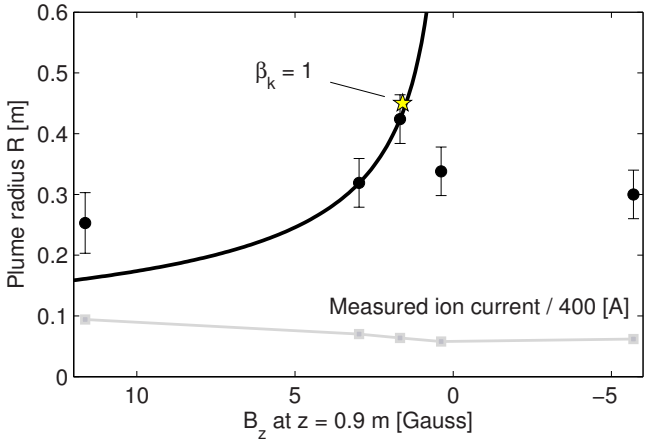

FIG. 10. (Color online) Plume width measurements at $z=0.9$ m for adjusted nozzle field. Data points (left to right) correspond to nozzle configurations 1, 3, 4, 5, and 6. Solid line is from Eq. (4) with ions tied to field lines. Plasma β_k at this position is less than unity for configurations 1 and 3, and 4. β_k is greater than unity for configurations 5 and 6.

by comparing with hydrogen at the same Mach number. Any acceleration or deceleration of the flow is obscured by measurement uncertainties.

B. Plasma flow in different magnetic configurations with He feed gas

Multiple nozzle coil configurations were tested to determine the nozzle's effect on plume width and detachment. Plume width was measured by the Langmuir triple-probe array at $z=0.9$ m under five different magnetic nozzle conditions using identical shots with helium input gas. The plasma source was operated in a lower power discharge mode for these helium discharges. A 0.4 Ω power limiting resistor was placed in line with the discharge capacitor reducing the peak current to 350 A, which increased the discharge time to 15 ms.

Nozzle coil currents were adjusted from the high-field configuration 1 to the negative, cusp configuration 6, resulting in a centerline magnetic field between $B_z=12$ G and $B_z=-5.7$ G at the $z=0.90$ m measurement location. It should be noted that in the case of negative centerline magnetic fields, lines of constant magnetic flux that pass through the plasma source do not pass through the downstream measurement region. This separation of the two magnetic zones is due to the magnetic cusp from the reversed nozzle coil currents. If plasma density were to exclusively follow the cusp magnetic field lines, there would be no ion current recorded at these downstream positions.

Measured plume widths R and total ion current I_i for five magnetic nozzle configurations are shown in Fig. 10. Expected plume widths based on the magnetic field scaling of Eq. (4) is also shown using the measured condition of nozzle configuration "3"as a reference. The total ion current increases slightly with applied field, and plume width ceases to follow magnetic field scaling as B_z becomes negative. Measurements of β_k for the five different configurations shows that centerline $\beta_k>1$ at $z=0.9$ m only for the two most negative field configurations, "5" and 6, while $\beta_k<1$ for configurations 1, 3, and "4." We conclude from the multiple nozzle configurations that a significant negative magnetic field in the region of magnetic detachment had little effect on the plasma flow, while an increase in magnetic nozzle field strength resulted in a narrower plume at this measurement location.

We compared two shots with very different nozzle configurations—zero nozzle current 3 and cusp configuration 6, as shown in Fig. 2. Configuration 3 has $B_z=3$ G at $z=0.90$ m, while configuration 6 has axial magnetic field $B_z=-5.7$ G at the same location. We measured line-integrated electron density at two locations, $z=0.33$ and 1.85 m. Line-integral electron density was measured with the 15 GHz interferometer at $z=1.85$ m, and the plume width R was estimated by comparing the centerline interferometer measurement with a second vertically offset interferometer measurement at $y=-0.3$ m. Velocity measurements for these two shots remained the same within experimental uncertainty—around 15 km/s. Despite the markedly different magnetic field profiles of configurations 3 and 6, the downstream plume diameters and densities remain the same, as is shown in Fig. 11, within measurement uncertainty that indicating the plasma flow is detached from the applied magnetic field at the downstream position.

IV. DISCUSSION

Axial scans of flux profiles (Figs. 5–8) clearly show that the plume flow is attached to the applied magnetic field until $\beta_k=1$ position on centerline, and after the $\beta_k=1$ position, the flow exhibits a ballistic trajectory. The ballistic trajectory would be expected from a plume that is no longer influenced by the applied magnetic fields. The observed ion flow velocity is constant to within error limits, and the total ion current is conserved over the length of the experiment. With a large number of charge exchange collisions, the flow velocity would have decreased leading to an increase in electron density. Recombination of electrons and ions at these densities is a slow process and cannot be important since the ion current remains constant. We conclude that the plasma has clearly detached from the applied magnetic field and that the plasma detachment takes place around the point where $\beta_k=1$.

Further evidence for plasma detachment comes from the comparison of two very different magnetic field conditions in Fig. 11. If the plasma flow had been confined by the applied fields in the reversed field configuration, a very low plasma density would have been seen at the downstream interferometer ($z=1.85$ m). The fact that nearly the same density was seen with the cusp field as in a similar discharge with gradually decreasing magnetic field confirms that the bulk of plasma plume is detached from the applied field.

Although detachment of the plume appears to be consistent with MHD theory, we should also consider whether detachment can occur when the ion cyclotron orbits $r_{ci}=\sqrt{kT_i m_i}/eB$ become larger than the plasma radius $R(z)$, as suggested in Ref. 5. For the experiments discussed earlier in hydrogen, the position where the ion cyclotron radius and the plume radius are nearly the same is at $z=0.81$ m. This position is close to the position where $\beta_k=1$. However electrons

Downloaded 16 Apr 2009 to 128.83.61.67. Redistribution subject to AIP license or copyright; see http://pop.aip.org/pop/copyright.jsp

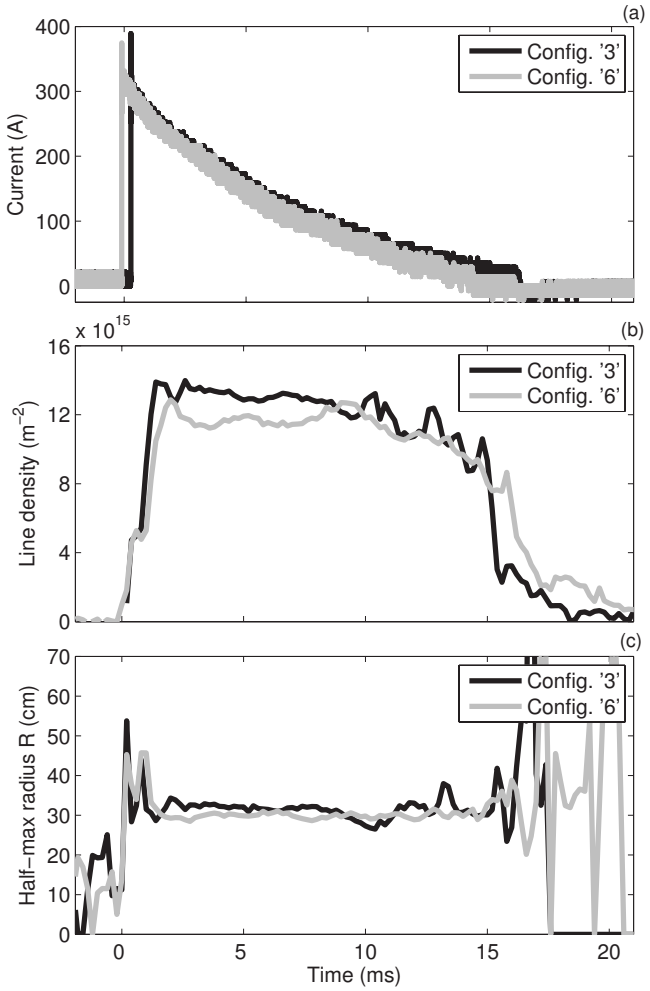

FIG. 11. (a) Plasma source current for a 300 V discharge voltage and He feed gas. (b) 15 GHz interferometer measurement at $z=1.85$ m. Line integral density was the same within shot-shot variation and 15% uncertainty for the two magnetic configurations. (c) Plume half-maximum radius measured at $z=1.85$ m. The plume radius for both magnetic configurations was 32 ± 5 cm. Config. 3 and Config. 6 refer to the magnetic field configuration, listed in Table I.

should still be attached to the applied field and ions would be confined by electrostatic fields from electrons over the Debye length. For the plasma conditions around the detachment point, the Debye length is about 10 μm, which is much smaller than plasma dimensions. For the experiments in helium, the location where the ion cyclotron radius is equal to the plume radius is at $z=0.54$ m. The flux measurements in Fig. 7 do not show any deviation from frozen flow until $z\sim0.8$ m, indicating a flow along the magnetic field where the magnetized electrons continued to confine the ions. Thus, the flux data in Fig. 7 are consistent with a detachment at $\beta_k=1$ rather than a detachment due to ion orbit effects.

We have also compared our measurements with a numerical MHD plasma detachment model for steady-state flow.[28] This code assumes a steady-state collisionless plasma, and ions with directed energy $\varepsilon=m_i v_z^2/2$. The initial conditions for the model input were the experimentally determined hydrogen density profile and velocity at $z=0.33$ m. The magnetic field of configuration 2 is chosen as an initial vacuum magnetic field. The Vlasov–Maxwell equations are

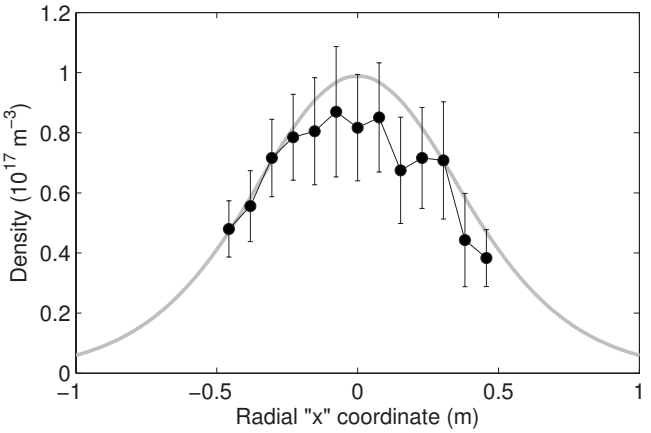

FIG. 12. Experimentally determined electron density radial profile at $z=1.85$ m (dots) compared to MHD simulation results (gray line). Experimental results are from interferometer-compensated Langmuir probe measurements.

then iteratively solved, seeking equilibrium magnetic fields resulting from the superposition of externally applied magnetic nozzle currents and self-consistent plasma currents. In Fig. 12 we compare the experimentally determined plasma density at $z=1.85$ with the simulated plasma density at the same location. The experimental electron density profile was reduced from Langmuir probe flux measurements normalized with a line averaged density from the interferometer at that location. Within the experimental accuracy there is agreement between simulations and experiment.

V. SUMMARY

This experiment provided detailed measurements of a magnetized plasma plume exiting a magnetic nozzle and detaching from the magnetic field. That is, the vacuum magnetic field has decreased by a factor of 100 over the range of our measurements and the plume continued with a nearly constant ion current. All measurements exhibited a constant flow velocity. Measured flux profiles were consistent with magnetically guided flow in the sub-Alfvenic part of the plume ($\beta_k<1$) and they deviated from the applied magnetic field lines in the super-Alfvenic part ($\beta_k>1$). A reversed field configuration was also tested, showing negligible change in plasma flux compared with a control configuration, highlighting the detachment of the plume from applied magnetic fields. We have demonstrated the detachment of a flowing magnetized plasma from the magnetic field. Numerical MHD simulations were also conducted showing good agreement with experimentally determined density profiles, in agreement with MHD detachment theory.[3]

ACKNOWLEDGMENTS

This work was supported in part by a NASA Graduate Student Researchers Program fellowship and financial support of the Ad Astra Rocket Co. to C. A. Deline. Dissertation and technical support was provided to Deline by his thesis advisor, B. Gilchrist, at the University of Michigan. The work at The University of Texas at Austin, University of Alabama at Huntsville and Marshall Space Flight Center was

Downloaded 16 Apr 2009 to 128.83.61.67. Redistribution subject to AIP license or copyright; see http://pop.aip.org/pop/copyright.jsp

supported by NASA under Contract No. NNJ05HB77C. Special thanks go to A. Arefiev and J. Meyer at the University of Texas for technical and analytical support. The authors would also like to thank M. LaPointe for numerous helpful comments.

[1]R. A. Gerwin, G. J. Marklin, A. G. Sgro, and A. H. Glasser, LANL Technical Report No. AL-TR-89–092, 1990. (See National Technical Information Service Document No. DE00763033 (R. A. Gerwin, G. J. Marklin, A. G. Sgro, and A. H. Glasser, LANL, Los Alamos, NM, AFOSR Technical Report AL-TR-89–092, 1990. (Copies may be ordered from National Technical Information Service, Springfield, VA.).
[2]E. B. Hooper and J. Propul, Power **9**, 757 (1993).
[3]A. V. Arefiev and B. N. Breizman, Phys. Plasmas **12**, 043504 (2005).
[4]E. N. Parker, Astrophys. J. **128**, 664 (1958).
[5]F. N. Gesto, B. D. Blackwell, C. Charles, and R. W. Boswell, J. Propul. Power **22**, 24 (2006).
[6]F. R. Chang Diaz, Fusion Technol. **35**, 87 (1999).
[7]M. West, C. Charles, R. Boswell, and J. Propul, Power **24**, 134 (2008).
[8]K. Toki, S. Shinohara, T. Tanikawa, and K. P. Shamrai, Thin Solid Films **506–507**, 597 (2006).
[9]V. B. Tikhonov, S. A. Semenikhin, J. R. Brophy, and J. E. Polk, *Proceedings of the 52th International Electric Propulsion Conference*, Cleveland, OH, August 1997 (Electric Rocket Propulsion Society, Cleveland, 1997), IEPC Paper No. 97-117.
[10]J. Squire, F. Chang-Diaz, M. Carter, L. Cassady, W. Chancery, T. Glover, V. Jacobson, G. McCaskill, R. Bengtson, E. Bering, and C. Deline, *Proceedings of the 30th International Electric Propulsion Conference*, Florence, Italy, September 2007 (Electric Rocket Propulsion Society, Cleveland, 1997), IEPC Paper No. 2007-181.
[11]G. Chavers, C. Dobson, J. Jones, M. Lee, A. Martin, J. Gregory, J. Cecil, R. Bengtson, B. Breizman, A. Arefiev, F. Chang-Diaz, J. Squire, T. Glover, G. McCaskill, J. Cassibry, and Z. Li, AIP Conf. Proc. **813**, 465 (2006).
[12]C. Deline, D. G. Chavers, and B. Gilchrist, *Proceedings of the 42nd Joint Propulsion Conference and Exhibit*, Sacramento, CA, July 2006 (American Institute of Aeronautics and Astronautics, Reston, 2006), AIAA Paper No. 2006-4653.
[13]G. Fiksel, A. F. Almagri, D. Craig, M. Lida, S. C. Prager, and J. S. Sarff, Plasma Sources Sci. Technol. **5**, 78 (1996).
[14]R. H. Jackson, IEEE Trans. Electron Devices **46**, 1050 (1999).
[15]S. L. Chen and T. Sekiguchi, J. Appl. Phys. **36**, 2363 (1965).
[16]R. Burton, S. DelMedico, J. C. Andrews, and J. Propul, Power **9**, 771 (1993).
[17]M. Walker, R. Hofer, and A. Gallimore, *Proceedings of the 38th Joint Propulsion Conference and Exhibit*, Indianapolis, IN, 2002 (American Institute of Aeronautics and Astronautics, Reston, 2006), AIAA Paper No. 2002-4253.
[18]C. Dobson, J. Jones, and D. G. Chavers, Rev. Sci. Instrum. **75**, 674 (2004).
[19]B. Gilchrist, S. Ohler, and A. Gallimore, Rev. Sci. Instrum. **68**, 1189 (1997).
[20]G. T. Whittaker and G. W. Watson, *A Course of Modern Analysis* (Cambridge University Press, Cambridge, 1902), p. 211.
[21]I. H. Hutchinson, *Principles of Plasma Diagnostics* (Cambridge University Press, Cambridge, 2002), p. 141.
[22]C. Deline, B. Gilchrist, C. Dobson, J. Jones, and G. Chavers, Rev. Sci. Instrum. **78**, 113504 (2007).
[23]H. Woo, K. Chung, Y. Choi, M. Lee, D. Zimmerman, and R. McWilliams, Contrib. Plasma Phys. **46**, 451 (2006).
[24]D. Tilley, A. Gallimore, A. Kelly, and R. Jahn, Rev. Sci. Instrum. **65**, 678 (1994).
[25]C. Deline, É. Choinière, and B. Gilchrist, "Assessment of plasma flow effect on Langmuir triple probe operation via kinetic simulation," IEEE Trans. Plasma Sci. (to be published).
[26]C. S. MacLatchy, C. Boucher, D. A. Poirier, and J. Gunn, Rev. Sci. Instrum. **63**, 3923 (1992).
[27]R. A. Spores, J. A. Pobst, J. H. Schilling, and D. A. Erwin, *Proceedings of the 28th Joint Propulsion Conference and Exhibit*, Nashville, TN, 1992 (American Institute of Aeronautics and Astronautics, Reston, 2006), AIAA Paper No. 92-3238.
[28]B. N. Breizman, M. R. Tushentsov, and A. V. Arefiev, Phys. Plasmas **15**, 057103 (2008).

Downloaded 16 Apr 2009 to 128.83.61.67. Redistribution subject to AIP license or copyright; see http://pop.aip.org/pop/copyright.jsp